



ORIGINAL ARTICLE

LncRNA-AK137033 inhibits the osteogenic potential of adipose-derived stem cells in diabetic osteoporosis by regulating Wnt signaling pathway via DNA methylation

Shuanglin Peng^{1,2,3} | Yujin Gao^{1,4,5} | Sirong Shi² | Dan Zhao² | Huayue Cao^{1,3,5} | Ting Fu^{1,3,5} | Xiaoxiao Cai²  | Jingang Xiao^{1,3,4,5} 

¹Department of Oral Implantology, The Affiliated Stomatology Hospital of Southwest Medical University, Luzhou, China

²State Key Laboratory of Oral Diseases, West China Hospital of Stomatology, Sichuan University, Chengdu, China

³National Key Clinical Specialty, The Affiliated Hospital of Southwest Medical University, Luzhou, China

⁴Orofacial Reconstruction and Regeneration Laboratory, The Affiliated Stomatology Hospital of Southwest Medical University, Luzhou, China

⁵Department of Oral and Maxillofacial Surgery, The Affiliated Stomatology Hospital of Southwest Medical University, Luzhou, China

Correspondence

Xiaoxiao Cai, State Key Laboratory of Oral Diseases, West China Hospital of Stomatology, Sichuan University, Chengdu 610041, China.

Email: dentistcai@hotmail.com

and.

Jingang Xiao, Department of Oral and Maxillofacial Surgery, The Affiliated Stomatology Hospital of Southwest Medical University, Luzhou 646000, China. Email: drxiaojingang@163.com

Funding information

National Natural Science Foundation of China, Grant/Award Number: 81870746 and 81970986; Open Project of the State Key Laboratory of Oral Disease Research, Grant/Award Number: SKLOD2021OF08; Joint project of Luzhou Municipal People's Government and Southwest Medical University, Grant/Award Number: 2020LZXNYDZ09;

Abstract

Objectives: Bone tissue engineering based on adipose-derived stem cells (ASCs) is expected to become a new treatment for diabetic osteoporosis (DOP) patients with bone defects. However, compared with control ASCs (CON-ASCs), osteogenic potential of DOP-ASCs is decreased, which increased the difficulty of bone reconstruction in DOP patients. Moreover, the cause of the poor osteogenesis of ASCs in a hyperglycemic microenvironment has not been elucidated. Therefore, this study explored the molecular mechanism of the decline in the osteogenic potential of DOP-ASCs from the perspective of epigenetics to provide a possible therapeutic target for bone repair in DOP patients with bone defects.

Materials and methods: An animal model of DOP was established in mice. CON-ASCs and DOP-ASCs were isolated from CON and DOP mice, respectively. AK137033 small interfering RNA (siRNA) and an AK137033 overexpression plasmid were used to regulate the expression of AK137033 in CON-ASCs and DOP-ASCs in vitro. Lentiviruses that carried shRNA-AK137033 or AK137033 cDNA were used to knockdown or overexpress AK137033, respectively, in CON-ASCs and DOP-ASCs in vivo. Hematoxylin and eosin (H&E), Masson's, alizarin red, and alkaline phosphatase (ALP) staining, micro-computed tomography (Micro-CT), flow cytometry, qPCR, western blotting, immunofluorescence, and bisulfite-specific PCR (BSP) were used to analyze the functional changes of ASCs.

Results: The DOP mouse model was established successfully. Compared with CON-ASCs, AK137033 expression, the DNA methylation level of the sFrp2 promoter region, Wnt signaling pathway markers, and the osteogenic differentiation potential were decreased in DOP-ASCs. In vitro experiments showed that AK137033 silencing inhibited the Wnt signaling pathway and osteogenic ability of CON-ASCs by reducing the DNA methylation level in the sFrp2 promoter region. Additionally, overexpression of AK137033 in DOP-ASCs rescued these changes caused by DOP. Moreover, the same results were obtained in vivo.

This is an open access article under the terms of the Creative Commons Attribution License, which permits use, distribution and reproduction in any medium, provided the original work is properly cited.

© 2021 The Authors. *Cell Proliferation* Published by John Wiley & Sons Ltd.

Youth Science Climbing Program of The Affiliated Stomatology Hospital of Southwest Medical University, Grant/Award Number: 2021KQ01; Project of Science & Technology Department of Sichuan Province, Grant/Award Number: 2018JY0399

Conclusions: LncRNA-AK137033 inhibits the osteogenic potential of DOP-ASCs by regulating the Wnt signaling pathway via modulating the DNA methylation level in the sFrp2 promoter region. This study provides an important reference to find new targets for the treatment of bone defects in DOP patients.

1 | INTRODUCTION

Diabetes mellitus (DM) is a systemic metabolic disease characterized by hyperglycemia. This systemic glucose metabolism disorder has a serious negative effect on the skeletal system by causing severe complications of the bone and joint system, ie, diabetic osteoporosis (DOP).^{1,2} In addition to the hyperglycemic microenvironment, DOP patients are also characterized by bone microstructure damage, bone strength reduction, fracture susceptibility, and bone defects that are not easily healed.³ For bone defects in DOP patients, the current treatment methods are not ideal.^{4,5} With the rapid development of tissue engineering, bone tissue engineering, which includes scaffold materials, seed cells, and growth factors, is considered to be the most promising method for bone defect repair.⁶ Adipose-derived stem cells (ASCs) are some of the most widely used seed cells in bone tissue engineering. However, our previous studies have shown that, compared with control adipose-derived stem cells (CON-ASCs), diabetic osteoporosis adipose-derived stem cells (DOP-ASCs) have less osteogenic potential,^{7,8} which limits their application to the treatment of fractures and bone defects in DOP patients. Therefore, the molecular mechanism of the osteogenic decline of DOP-ASCs requires further exploration to find potential therapeutic targets for the treatment of bone defects in DOP patients.

Wnt signaling pathways are a group of multifunctional signal transduction pathways activated by the binding of the Wnt ligand to the cell membrane receptor. They participate in various physiological and pathological processes of cells, which include various bone tissue diseases such as osteoporosis and stem cell-related bone regeneration.⁹ Activation of the Wnt signaling pathway in stem cells improves their ability of bone differentiation, whereas the inhibition of the Wnt signaling pathway reduces bone formation.^{10,11} Our previous studies have shown that the decrease in the osteogenic potential of DOP-ASCs compared with CON-ASCs is related to the Wnt signaling pathway.⁸ However, the molecular mechanism that underlies the regulation of the Wnt pathway for the osteogenic potential of DOP-ASCs is unclear.

Mammalian DNA methylation refers to methylation of the fifth carbon atom on cytosine in the CpG dinucleotide of DNA, which is catalyzed by four DNA methyltransferases, namely DNMT1, DNMT2, DNMT3a, and DNMT3b. It is generally believed that hypermethylation of DNA is related to the inhibition of gene expression, whereas DNA demethylation has the opposite effect.^{12,13} Because the promoter regions of many genes contain high-density CpG dinucleotide aggregation regions, namely CpG islands, DNA methylation plays an important role in mammalian cell biology.^{14,15} Recent studies have shown that DNA methylation may affect the multidirectional

differentiation of stem cells by regulating the expression of specific genes, which results in various bone diseases that include osteoporosis and osteoarthritis.^{16,17} Therefore, exploring DNA methylation provides a possibility to investigate novel molecular mechanisms of the osteogenic decline in DOP-ASCs.

Protein coding genes have been studied extensively, but they account for only 1.5% of the human genome.¹⁸ Noncoding RNAs (ncRNAs), which account for up to 98% of the genome, were once ignored. These ncRNAs are divided into long noncoding RNAs (LncRNAs) and short-chain ncRNAs in accordance with the transcript length. LncRNAs are a class of ncRNAs with transcript lengths longer than 200 bases, which are localized in the nucleus or cytoplasm.^{19,20} With the gradual deepening of the research on LncRNAs, many studies have reported that LncRNAs regulate gene expression at the epigenetic, transcriptional, and post-transcriptional levels, and have a potential regulatory effect on the cell fate of mesenchymal stem cells and the occurrence and development of specific diseases.^{19,21,22} In particular, studies have confirmed that LncRNAs affect the expression of specific genes by regulating the DNA methylation level in their promoter region.²³⁻²⁵ However, the molecular mechanism of LncRNAs in regulating the osteogenic differentiation and bone regeneration of DOP-ASCs is unclear. Therefore, an epigenetic mechanism, such as the regulation of LncRNAs or DNA methylation in the osteogenic ability of DOP-ASCs, has become a possible explanation for the decline in the osteogenic potential of DOP-ASCs.

In the present study, we subjected CON-ASCs and DOP-ASCs to mRNA/LncRNA expression profiling and MeDIP sequencing. The results showed a significant difference in the DNA methylation level of the promoter region of the Wnt signaling molecule sFrp2, which was related to LncRNA-AK137033. Subsequently, we conducted functional studies of sFrp2 and LncRNA-AK137033 in vivo and in vitro to explore the molecular mechanism that regulates bone differentiation of DOP-ASCs from the perspective of epigenetics.

2 | MATERIALS AND METHODS

2.1 | Diabetic osteoporosis animal model

All procedures related to animal experiments were reviewed and approved by the Ethics Committee of Southwest Medical University (20180391222) and carried out in accordance with the guidelines of the Care and Use of Laboratory Animals (Ministry of Science and Technology of China, 2006). Four-week-old male C57BL/6 mice were purchased from the Experimental Animal Center of Southwest Medical University. Fifty mice were randomly divided into CON and

DOP groups. The CON group was fed an ordinary diet, and the DOP group was fed a high fat and sugar (HFS) diet. The HFS diet consisted of 65% standard chow, 10% fat, 20% sucrose, 2.5% cholesterol, and other necessary additives (BIOG, Beijing, China). The weight and blood glucose of mice were measured every week. After 4 weeks, 50 mice were fasted for 12 h, followed by injection of streptozotocin (STZ; Sigma, St Louis, USA) in the DOP group (140 mg/kg) or the same volume of citric acid-sodium citrate buffer (140 ml/kg) in the CON group. After the injection, CON mice were raised on standard chow and DOP mice were still raised on the HFS diet. Additionally, all mice were fed under appropriate conditions (20–25°C with 65%–80% humidity) with free access to drinking water and food. The blood glucose and body weight of each group of mice were recorded every 3–5 days. After 4 months of feeding, the diabetic osteoporosis model was established. Until the end of the study, the mortality rate of STZ-induced diabetic osteoporosis mice was 20%–33%.

2.2 | Hematoxylin and eosin (H&E), and Masson's staining

Samples were fixed in 10% paraformaldehyde for 24 h, decalcified in a decalcification solution for about 1 month (this step was omitted for soft tissue), washed with tap water for 48 h, dehydrated with an alcohol gradient, embedded in paraffin, and sectioned. The samples were then stained with H&E and Masson's dye.

2.3 | Micro-CT analysis

Samples were fixed with 10% paraformaldehyde for 24 h and then analyzed by a SCANCO Medical CT-40 (SCANCO Medical, Bassersdorf, Switzerland). Scanning parameters were as follows: voltage, 80 kV; current, 500 μ A; exposure time, 200 ms; rotation angle, 220°; CT reconstruction method; and COBRA-filtered back-projection reconstruction.

2.4 | Isolation and culture of CON-ASCs and DOP-ASCs

CON-ASCs and DOP-ASCs were obtained from inguinal subcutaneous adipose tissue of CON and DOP mice, respectively. An adipose block from the groin was cut into pieces of about 1 mm³ and evenly spread in a T25 culture flask. After covering the cap tightly, the flask was turned upside down and incubated at 37°C for about 5 min. Then, α -modified Eagle's medium (Hyclone, Pittsburgh, USA) with 10% FBS (Schaumburg, USA) was carefully added to the culture flask to completely immerse the tissue blocks. Subsequently, the tissue blocks were incubated at 37°C with 5% CO₂ for 7–10 days to obtain passage 0 cells. The cells were passaged at 80%–90% confluence, and passage 3 cells were used in experiments.

TABLE 1 Primer sequences for qPCR amplification of specific genes

Genes	Sequence (5'→3')
<i>Gapdh</i>	
Forward	GGTGAAGGTCGGTGTGAACG
Reverse	CTCGCTCTGGAAGATGGTG
<i>AK137033</i>	
Forward	GCATGTACCCACATTTTCAGC
Reverse	CCAGCAATACACAGCAGGAC
<i>sFrp2</i>	
Forward	CGTGGGCTTCTCTCTTCG
Reverse	ATGTTCTGGTACTCGATGCCG
<i>β-Catenin</i>	
Forward	GCTGCGTGGACAATGGCTACTC
Reverse	AGCGTCAAACGCGTGGATGG
<i>Opn</i>	
Forward	TCCCTCCCGGTGAAAGTGACTG
Reverse	TCCTCGCTCTCTGCATGGTCTC
<i>Runx2</i>	
Forward	GACTGTGGTTACCGTCATGGC
Reverse	ACTTGGTTTTTCATAACAGCGGA

2.5 | Characterization of isolated ASCs by flow cytometry

Passage 3 ASCs was resuspended with PBS and stained for CD29, CD44, CD45, CD90, CD31, or CD34 with fluorophore-conjugated antibodies at 4°C for 30 min. Unstained cells were used as a blank control. After washing with PBS, the cells were analyzed using a FACS Calibur flow cytometer (BD Biosciences, San Jose, USA).

2.6 | Quantitative polymerase chain reaction

Quantitative polymerase chain reaction (qPCR) was used to measure the mRNA expression levels of *AK137033*, secreted frizzled-related protein 2 (*sFrp2*), cadherin-associated protein, delta 1 (*β -catenin*), osteopontin (*Opn*), and runt-related transcription factor 2 (*Runx2*) in ASCs after osteogenic induction. Primer sequences are presented in Table 1. Total RNA from ASCs was extracted using an RNeasy Plus Mini kit (Qiagen, Hilden, Germany) in accordance with the manufacturer's instructions, and a PrimeScript RT reagent kit with gDNA Eraser (Takara Bio, Tokyo, Japan) was then used to synthesize cDNA from the total RNA. qPCR was performed using a SYBR Premix ExTaq kit (Takara Bio, Tokyo, Japan) and ABI 7300 system (Applied Biosystems, Wilmington, USA) in accordance with the manufacturers' instructions with the following parameters: 95°C for 30 s and then 45 cycles of 95°C for 5 s and 60°C for 34 s. Glyceraldehyde phosphate dehydrogenase (GAPDH) was used as the internal reference.²⁶

2.7 | Western blot analysis

Protein expression levels in ASCs after osteogenic induction were measured by western blotting. Total protein was extracted from ASCs using a total protein extraction kit (Keygen Biotech, Nanjing, China) in accordance with the manufacturer's instructions. Protein samples were mixed with loading buffer and boiled for 5 min for denaturation. After separation by SDS-PAGE, the protein samples were transferred to a polyvinylidene fluoride membrane by the wet transfer method and blocked in 5% dry skim milk at 37°C for 1 h. The blots were then incubated with diluted primary antibodies against sFrp2 (abs134753) (Absin, Shanghai, China), GSK-3 β (12456), p-GSK-3 β (5558) (Cell Signaling Technology, Danvers, USA), GAPDH (ab181602), β -catenin (ab32572), OPN (ab8448), or RUNX2 (ab92336) (Abcam, Cambridge, UK) with shaking at 4°C overnight. The following day, the membranes were washed three times with Tris-buffered saline with Tween-20 (TBST) and then incubated with diluted HRP-labeled goat anti-rabbit or anti-mouse secondary antibodies for 1 h. Then, the membranes were washed three times with TBST and developed with an enhanced chemiluminescence detection system (Bio-Rad, Hercules, USA).^{27,28}

2.8 | Immunofluorescence staining

Immunofluorescence staining was used to analyze the relative expression of RUNX2 and OPN protein in ASCs. CON-ASCs and DOP-ASCs after osteogenic induction were washed with PBS for three times, fixed with 4% paraformaldehyde for 30 min, and then permeabilized with 0.5% Triton X-100 for 10 min. Subsequently, the samples were incubated with 5% sheep serum at 37°C for 1 h and then incubated with diluted primary antibodies (anti-RUNX2 or -OPN) overnight. The following day, the samples were rewarmed at 37°C for 1 h and then incubated with a diluted fluorescent dye-conjugated anti-rabbit secondary antibody (Invitrogen, CA, USA) at 37°C for 1 h. The cytoskeleton and nucleus of ASCs were stained with phalloidin and 4'-diamidino-2-phenylindole, respectively. Fluorescence images of each sample were obtained under a confocal laser microscope (Nikon, Tokyo, Japan).^{29,30}

2.9 | Cell transfection

AK137033-specific SiRNA was synthesized by GenePharma (Shanghai, China), SiRNA sequences are shown in Table 2.

For AK137033 overexpression, the AK137033 cDNA sequence was amplified and subcloned into a pcDNA3.1 vector. An empty pGFP3.1 vector that carried eGFP was used as the negative control.

SiRNA and the plasmid were transfected into ASCs using the Auto Electroporator system (Bimake, TX, USA) in accordance with the manufacturer's instructions for in vitro experiments.

TABLE 2 SiRNA sequences designed for AK137033

	Sequence (5'→3')
SiRNA	
Sense	GCAUCAUGCAAUGAGGAAUTT
Antisense	AUCCUCAUUGCAUGAUGCTT
SiRNA-NC	
Sense	UUCUCCGAACGUGUCACGUTT
Antisense	ACGUGACACGUUCGGAGAATT

For AK137033-specific overexpression, lentivirus and shRNA lentivirus were synthesized by Obio Technology (Shanghai, China). For AK137033 overexpression, the AK137033 cDNA sequence was amplified and subcloned into the pSLenti-EF1-EGFP-F2A-Puro-WPRE2-CMV-MCS lentiviral vector. For AK137033 knockdown, oligonucleotides with AK137033 splice variant RNA interference targets were annealed and ligated into the pSLenti-U6-shRNA-CMV-EGFP-F2A-Puro-WPRE lentiviral vector. The oligonucleotide sequences of shRNA with AK137033 RNA interference targets are shown in Table 3.

AK137033 overexpression or AK137033 knockdown lentiviruses were transfected into ASCs in accordance with the manufacturer's instructions for in vivo experiments.

2.10 | Alizarin red and alkaline phosphatase (ALP) staining

After 3 or 5 days of osteoinduction, ASCs were rinsed with PBS three times and then fixed with 4% paraformaldehyde at 4°C for 30 min. ALP activity was detected by an Alkaline Phosphatase Assay Kit (Beyotime, Shanghai, China) in accordance with the manufacturer's guidelines. Similarly, after 14 days of osteoinduction, ASCs were rinsed with PBS for three times and then fixed with 4% paraformaldehyde at 4°C for 30 min. Fixed ASCs were incubated in a 0.1% alizarin red solution for 30 min at 37°C to assess the formation of calcium nodules.

2.11 | Preparation of ASC-seeded BCP scaffolds

Biphasic calcium phosphate (BCP) scaffolds were provided by Sichuan University Research Center. After autoclaving the scaffolds, ASCs infected with lentiviruses were seeded on BCP scaffolds at $2 \times 10^5/\text{cm}^2$ and cultured in osteogenic induction medium for 48 h for subsequent in vivo experiments.

2.12 | Establishment of a critical-sized calvarial bone defect model in mice and implantation of ASC-seeded BCP scaffolds in vivo

ASC-seeded BCP scaffolds were prepared as the following groups: BCP scaffold seeded with CON-ASCs (CON-B), BCP scaffold seeded with CON-ASCs transfected with the knockdown

TABLE 3 Oligonucleotide sequences of shRNAs with AK137033 RNA interference targets

	5'	STEM	Loop	STEM	3'
sh-AK137033-F	Ccgg	GGTCAACTACTACGTATAT	TTC AAGAGA	ATATACGTAGTAGTTGACC	TTTTTTg
sh-AK137033-R	aattcaaaaa	GGTCAACTACTACGTATAT	TCTCTTGAA	ATATACGTAGTAGTTGACC	
sh-NC-F	Ccgg	CCTAAGGTTAAGTCGCCCTCG	CTCGAG	CGAGGGCGACTTAACCTTAGG	TTTTTTg
sh-NC-R	aattcaaaaa	CCTAAGGTTAAGTCGCCCTCG	CTCGAG	CGAGGGCGACTTAACCTTAGG	

lentiviral vector (CON-NC), BCP scaffold seeded with CON-ASCs with AK137033 knockdown (CON-shRNA), BCP scaffold seeded with DOP-ASCs (DOP-B), BCP scaffold seeded with DOP-ASCs infected with the overexpression lentiviral vector (DOP-NC), and BCP scaffold seeded with DOP-ASCs overexpressed AK137033 (DOP-LVRNA). Fifteen CON mice were randomly divided into three groups, and fifteen DOP mice were randomly divided into three groups. A circular defect of 4 mm in diameter was made on the right calvarium of each mouse under sterile conditions. The prepared scaffolds were implanted into the bone defects (five mice in each group), and then, the muscle layer and skin were sutured. After the operation, the mice were fed under appropriate conditions (20–25°C with 65%–80% humidity).

2.13 | Statistical analysis

SPSS 19.0 software was used for statistical analysis. Data were tested by the t-test or one-way analysis of variance. Each experiment was repeated at least three times. The results are expressed as the mean \pm standard deviation (SD). Data were significantly different at $p < 0.05$.

3 | RESULTS

3.1 | Successful establishment of the diabetic osteoporosis animal model

After STZ injection, we continuously observed changes in body weight and blood glucose in mice. The blood glucose levels of CON mice were <9 M; the blood glucose levels of mice in the DOP group were maintained at >16.8 M; and the weight of mice in the DOP group was lower than that in the CON group (Figure 1A). Compared with the CON group, H&E and Masson's staining of the pancreas showed that the volume of islets tissue in the DOP group was smaller, vacuolar degeneration had occurred, and inflammatory cells had infiltrated around islets (Figure 1B). The femurs of CON and DOP mice were stained with H&E and Masson, and subjected to micro-CT at 4 months after STZ injection. The results of histochemical staining showed that, compared with the CON group, bone trabeculae were fewer and disordered in the DOP group, and the bone cortex had become thinner (Figure 1C). These results were confirmed by micro-CT analysis (Figure 1D). Compared with CON mice, statistical analysis

showed that Tb.BV/TV and Tb. Th were decreased, but Tb.BS/BV had increased in DOP mice (Figure 1E). On the basis of the above results, we concluded that the DOP mice model was established successfully.

3.2 | Successful isolation and culture of CON-ASCs and DOP-ASCs, and their LncRNA/mRNA expression profiles

CON-ASCs and DOP-ASCs were obtained from CON mice and DOP mice, respectively. The ASCs of each passage were observed under an inverted phase contrast microscope. Cell culture showed that ASCs grew adherently and were spindle shaped, plump, and distributed evenly (Figure 2A). The surface antigens of the passage 3 ASCs were detected by flow cytometry. Surface antigens CD29, CD44, and CD90 were positive on CON-ASCs and DOP-ASCs, and CD31, CD34, and CD45 were negative (Figure 2B, C). These results indicated that the ASCs were highly pure. Compared with CON-ASCs, cluster and volcano plots of LncRNA/mRNA expression profiles revealed that 370 LncRNAs and 362 mRNAs were upregulated, and 256 LncRNAs and 152 mRNAs were downregulated in DOP-ASCs (fold change > 1.5 , and $p < 0.05$) (Figure 2D, E).

3.3 | Expression of AK137033, the Wnt signaling pathway, and osteogenic differentiation potential are downregulated in DOP-ASCs

After 3 days of osteogenic induction, western blotting was used to measure the protein levels of sFrp2, GSK-3 β , p-GSK-3 β , β -catenin, RUNX2, and OPN in CON-ASCs and DOP-ASCs. Moreover, the mRNA levels of AK137033, β -Catenin, Runx2, and Opn were measured by qPCR. Additionally, ALP and alizarin red staining was used to detect differences in the osteogenic abilities of CON-ASCs and DOP-ASCs after 3 and 14 days of osteogenic induction. Compared with CON-ASCs, the protein and gene expression levels of Wnt signaling pathway makers and osteogenesis-related molecules, and the expression of LncRNA-AK137033 were downregulated in DOP-ASCs (Figure 3A, B). Moreover, ALP and alizarin red staining revealed fewer alkaline phosphatase and mineralized nodules in the DOP group than in the CON group (Figure 3C). These results showed that the expression of AK137033, the Wnt signaling pathway, and osteogenic differentiation potential were downregulated in DOP-ASCs.

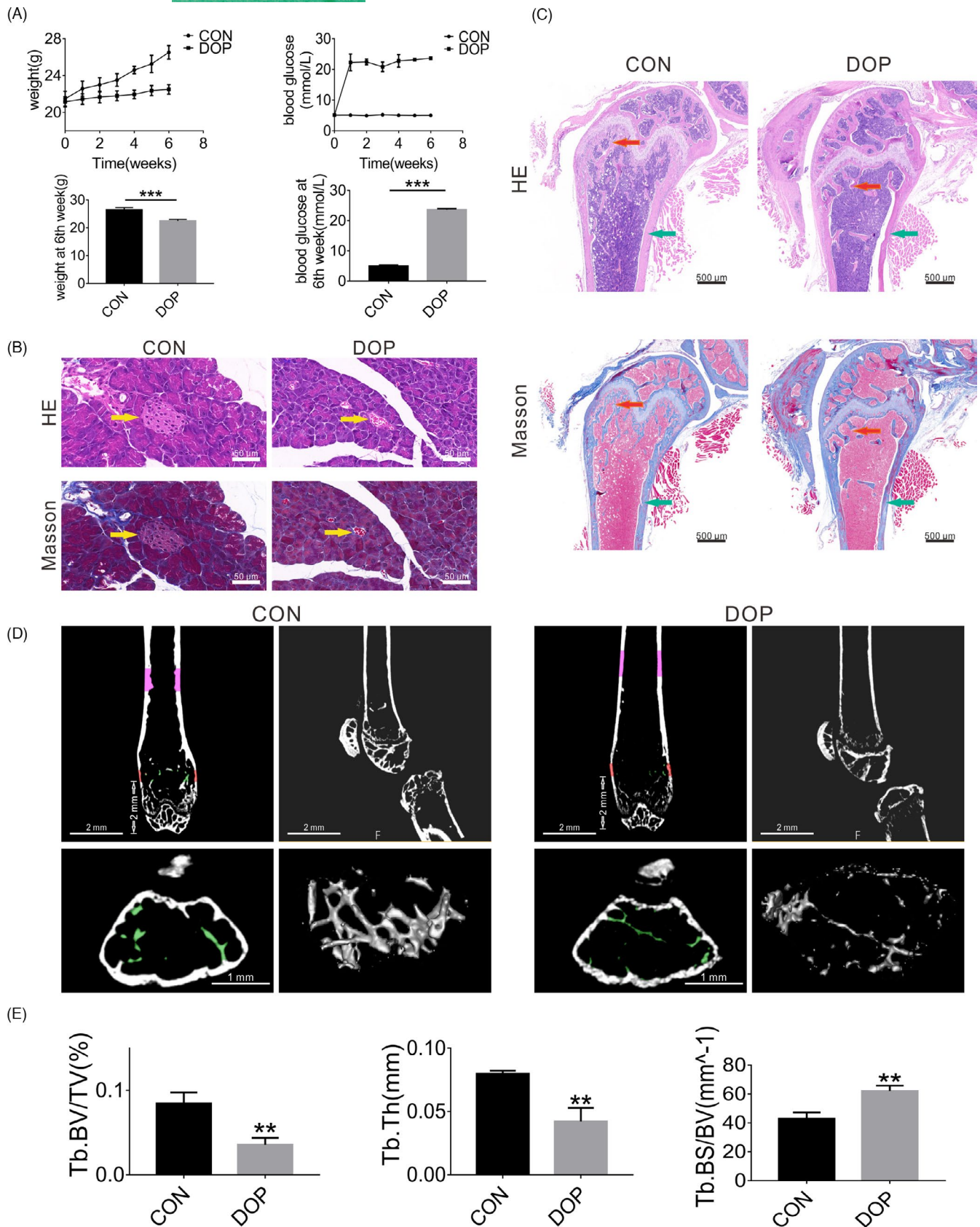


FIGURE 1 Successful establishment of the diabetic osteoporosis mouse model. A, Compared to CON mice, DOP mice had a lighter body weight and higher blood glucose level (>16.8 M). B, The volume of islet tissue in the DOP group was smaller, vacuolar degeneration had occurred, and inflammatory cells had infiltrated around islets (indicated by yellow arrows). C, D, Histochemical staining and micro-CT analysis showed that, compared with the femur of the CON group, there was less and disordered bone trabeculae in the DOP group (indicated by red arrows) and the bone cortex had become thinner (indicated by green arrows). E, Statistical analysis of Tb.BV/TV, Tb.Th, and Tb.BS/BV between CON and DOP mice. Data shown as the mean \pm SD ($n \geq 3$), $*p < 0.05$; $**p < 0.01$; $***p < 0.001$

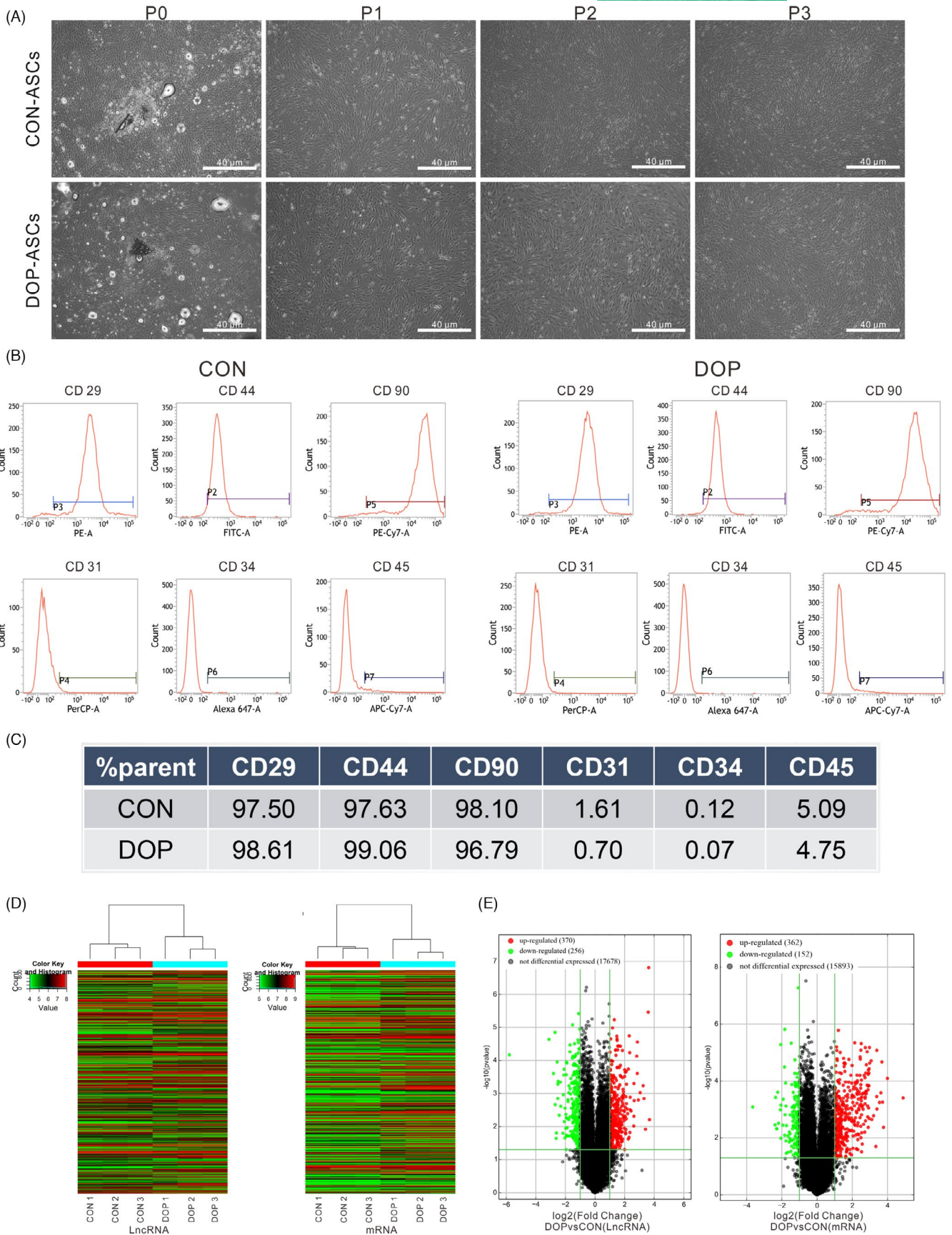


FIGURE 2 Isolation and culture of CON-ASCs and DOP-ASCs, and the results of LncRNA/mRNA expression profiling. A, Normal appearance of CON-ASCs and DOP-ASCs observed under an inverted phase contrast microscope. B, C, Surface antigens of passage 3 ASCs detected by flow cytometry. D, E, Cluster and volcano plots of LncRNA/mRNA expression profiles

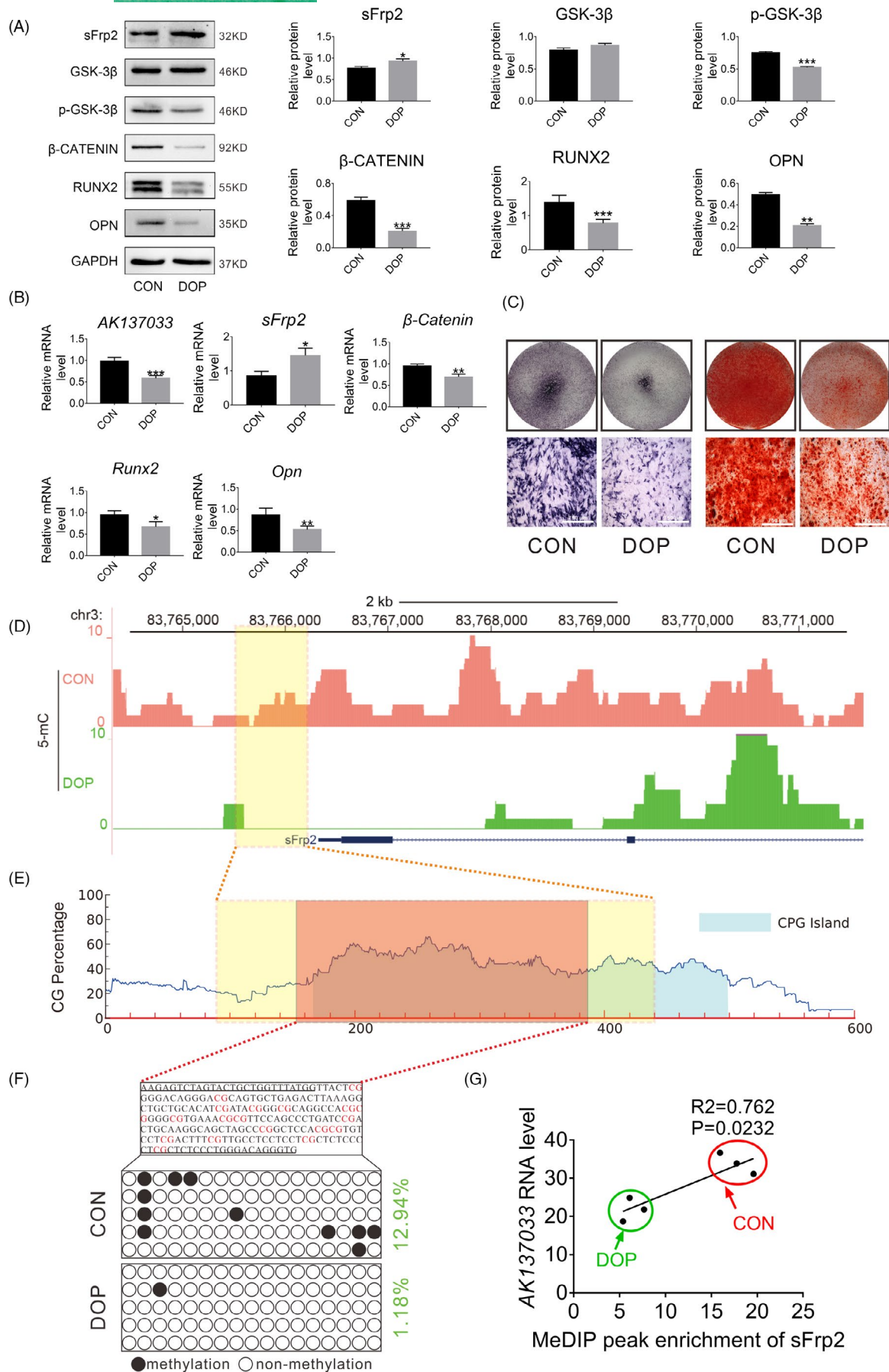


FIGURE 3 AK137033 and a change in the methylation levels of the sFrp2 promoter region are involved in the regulation of the osteogenic differentiation potential of DOP-ASCs. A, Western blot analysis of sFrp2, p-GSK-3 β , β -catenin, RUNX2, and OPN in CON-ASCs and DOP-ASCs. B, qPCR analysis of AK137033, sFrp2, β -Catenin, Runx2, and Opn in CON-ASCs and DOP-ASCs. C, ALP and alizarin red staining revealed less alkaline phosphatase activity and fewer mineralized nodules in the DOP group than those in the CON group. D, MeDIP sequencing showed that the DNA methylation level of the sFrp2 promoter region in DOP-ASCs was significantly higher than that in CON-ASCs (genomic coordinates: chr3, 83765880–83766230). E, Meth Primer analysis showed a large amount of CpG islands (CGIs) in the sFrp2 promoter region (genomic coordinates: chr3, 83765880–83766230). F, BSP confirmed that the methylation level in the sFrp2 promoter region (genomic coordinates: chr3, 83765880–83766230) of CON-ASCs was higher than that in DOP-ASCs. G, Correlation analysis of AK137033 and the DNA methylation level of the sFrp2 promoter region in CON-ASCs and DOP-ASCs. Data shown as the mean \pm SD ($n \geq 3$), * $p < 0.05$; ** $p < 0.01$; *** $p < 0.001$

3.4 | Inhibition of the Wnt signaling pathway in DOP-ASCs may be related to AK137033 and changes in the DNA methylation level in the sFrp2 promoter region

We performed MeDIP sequencing and mRNA/LncRNA expression profiling of CON-ASCs and DOP-ASCs. MeDIP sequencing showed that the DNA methylation peak of the sFrp2 promoter region in CON-ASCs was significantly higher than that in DOP-ASCs (genomic coordinates: chr3, 83765880–83766230) (Figure 3D). Interestingly, calculation by Meth Primer software showed a large amount of CpG islands (CGIs) in the sFrp2 promoter region (genomic coordinates: chr3, 83765880–83766230), which is a prerequisite for DNA methylation (Figure 3E). BSP results confirmed that the methylation degree of CON-ASCs was higher than that of matched DOP-ASCs in the sFrp2 promoter region (genomic coordinates: chr3, 83765880–83766230) (Figure 3F). Additionally, combined with the results of MeDIP sequencing and mRNA/LncRNA expression profiling, we found a statistical correlation between AK137033 expression and the methylation level in the sFrp2 promoter region (Figure 3G). These results demonstrated that the inhibition of the Wnt signaling pathway in DOP-ASCs may be related to AK137033 and changes in the DNA methylation level in the sFrp2 promoter region.

3.5 | AK137033 silencing inhibits the Wnt signaling pathway in CON-ASCs by reducing the DNA methylation level of the sFrp2 promoter region

Previous studies have shown that the inhibition of the Wnt signaling pathway in DOP-ASCs may be related to AK137033 and changes in the DNA methylation level in the sFrp2 promoter region, and AK137033 was highly expressed in CON-ASCs. Therefore, we silenced AK137033 by specific siRNAs in CON-ASCs and then detected the expression of mRNAs and proteins related to the Wnt signaling pathway. CON-ASCs in the siRNA group were transfected with si-AK137033, and CON-ASCs in groups B and NC were treated with ordinary osteogenic induction medium and a siRNA negative control, respectively. At 3 days after osteogenic induction, we performed qPCR and western blot analyses. Compared with B and NC groups, the Wnt signaling pathway markers and downstream osteogenesis-related molecules in the siRNA group were suppressed after AK137033 silencing (Figure 4A, B). Similar results were obtained after 5 days of osteogenesis induction

(Figure 4C, D). More importantly, BSP results revealed that the DNA methylation level of the sFrp2 promoter region in the siRNA group was downregulated after AK137033 silencing (Figure 4E). These changes indicated that AK137033 silencing inhibited the Wnt signaling pathway in CON-ASCs by reducing the DNA methylation level of the sFrp2 promoter region.

3.6 | AK137033 silencing decreases the osteogenic ability of CON-ASCs cells

To explore changes in the osteogenic differentiation potential after silencing AK137033 in CON-ASCs, we performed immunofluorescence, alizarin red, and ALP staining. At 3 days after osteogenic induction, immunofluorescence staining showed that the expression of RUNX2 and OPN in the siRNA group was decreased compared to that in B and NC groups (Figure 5A, B). Alizarin red staining revealed fewer mineralized nodules in the siRNA group than in B and NC groups after 14 days of osteogenic induction (Figure 5C). At 3 and 5 days of osteogenic induction, ALP staining showed less alkaline phosphatase produced by the siRNA group than that by B and NC groups (Figure 5D, E). These results suggested that silencing AK137033 reduced the osteogenic differentiation potential of CON-ASCs.

3.7 | AK137033 overexpression activates the Wnt signaling pathway in DOP-ASCs by increasing the DNA methylation level of the sFrp2 promoter region

At 3 days after osteogenic induction, compared with B and NC groups, qPCR and western blotting showed that the mRNA and protein levels of Wnt signaling pathway markers and downstream osteogenesis-related molecules were increased in the AK137033 plasmid (OE) group (Figure 6A, B). Similar results were obtained after 5 days of osteogenic induction (Figure 6C, D). Additionally, BSP results showed that the DNA methylation level of the sFrp2 promoter region in the OE group was increased after AK137033 overexpression (Figure 6E). To activate the Wnt signaling pathway in DOP-ASCs, we transfected a plasmid that carried the AK137033 cDNA sequence into DOP-ASCs (Figure 6F). Taken together, these observations indicated that AK137033 overexpression activated the Wnt signaling pathway in DOP-ASCs by increasing the DNA methylation level of the sFrp2 promoter region.

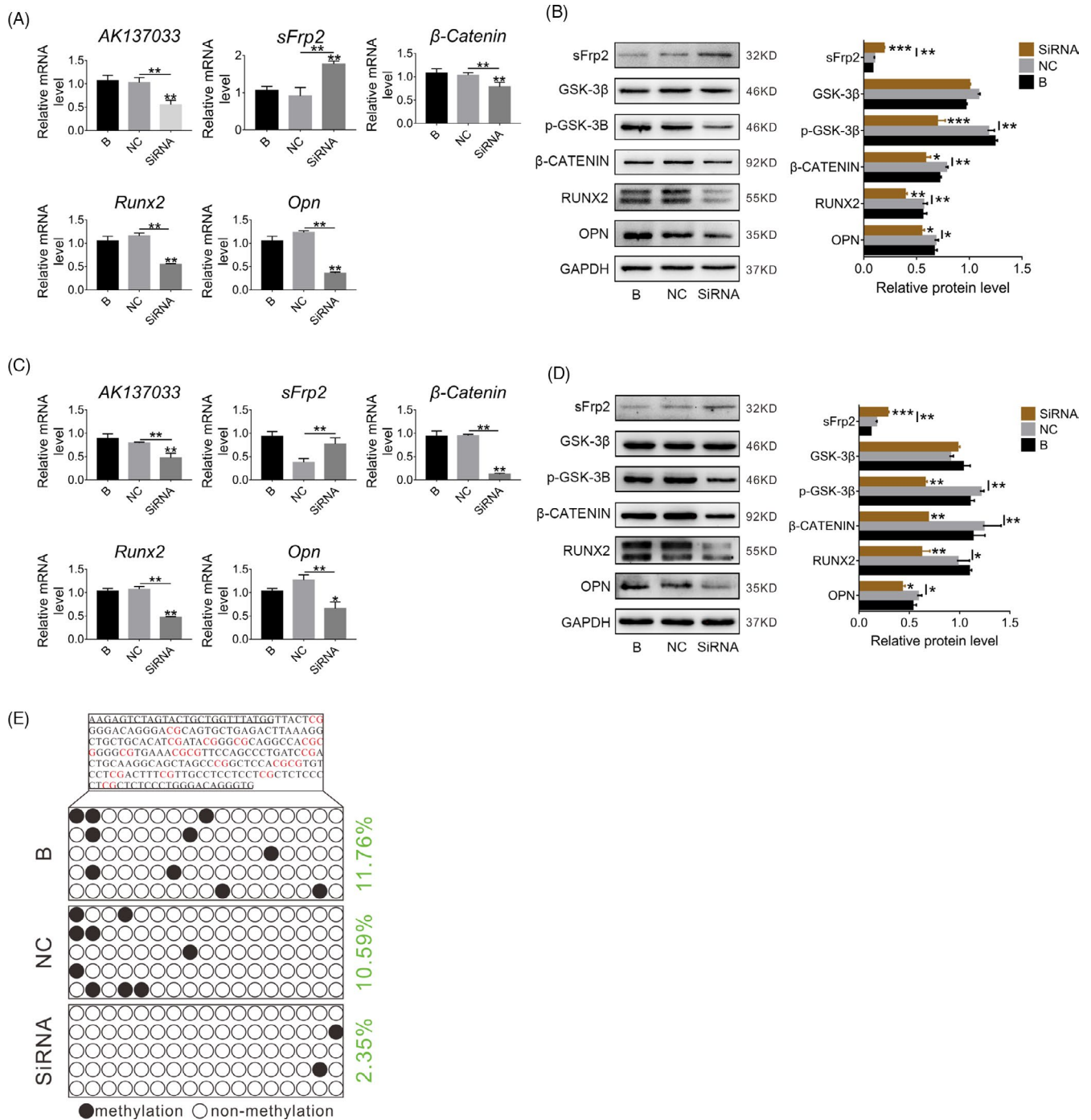


FIGURE 4 AK137033 silencing inhibits the Wnt signaling pathway in CON-ASCs by reducing the DNA methylation level of the sFrp2 promoter region. A, B, The mRNA and protein levels of Wnt signaling pathway makers and osteogenesis-related molecules in the SiRNA group were decreased after AK137033 silencing in CON-ASCs (osteoinduction for 3 days). C, D, After AK137033 was silenced in CON-ASCs, the mRNA and protein levels of Wnt signaling pathway markers and osteogenesis-related molecules were decreased in the SiRNA group (osteoinduction for 6 days). E, BSP results revealed that the DNA methylation level of the sFrp2 promoter region in the SiRNA group was downregulated compared with that in B and NC groups. Data shown as the mean \pm SD ($n \geq 3$), * $p < 0.05$; ** $p < 0.01$; *** $p < 0.001$

3.8 | AK137033 overexpression increases the osteogenic ability of DOP-ASCs

To investigate changes in the osteogenic differentiation potential of DOP-ASCs after overexpression of AK137033, immunofluorescence,

alizarin red, and ALP staining were performed. After 3 days of osteogenic induction, immunofluorescence staining showed that the expression of RUNX2 and OPN in the OE group was increased compared with that in B and NC groups (Figure 7A, B). Alizarin red staining showed more mineralized nodules in the OE group than those in B and NC

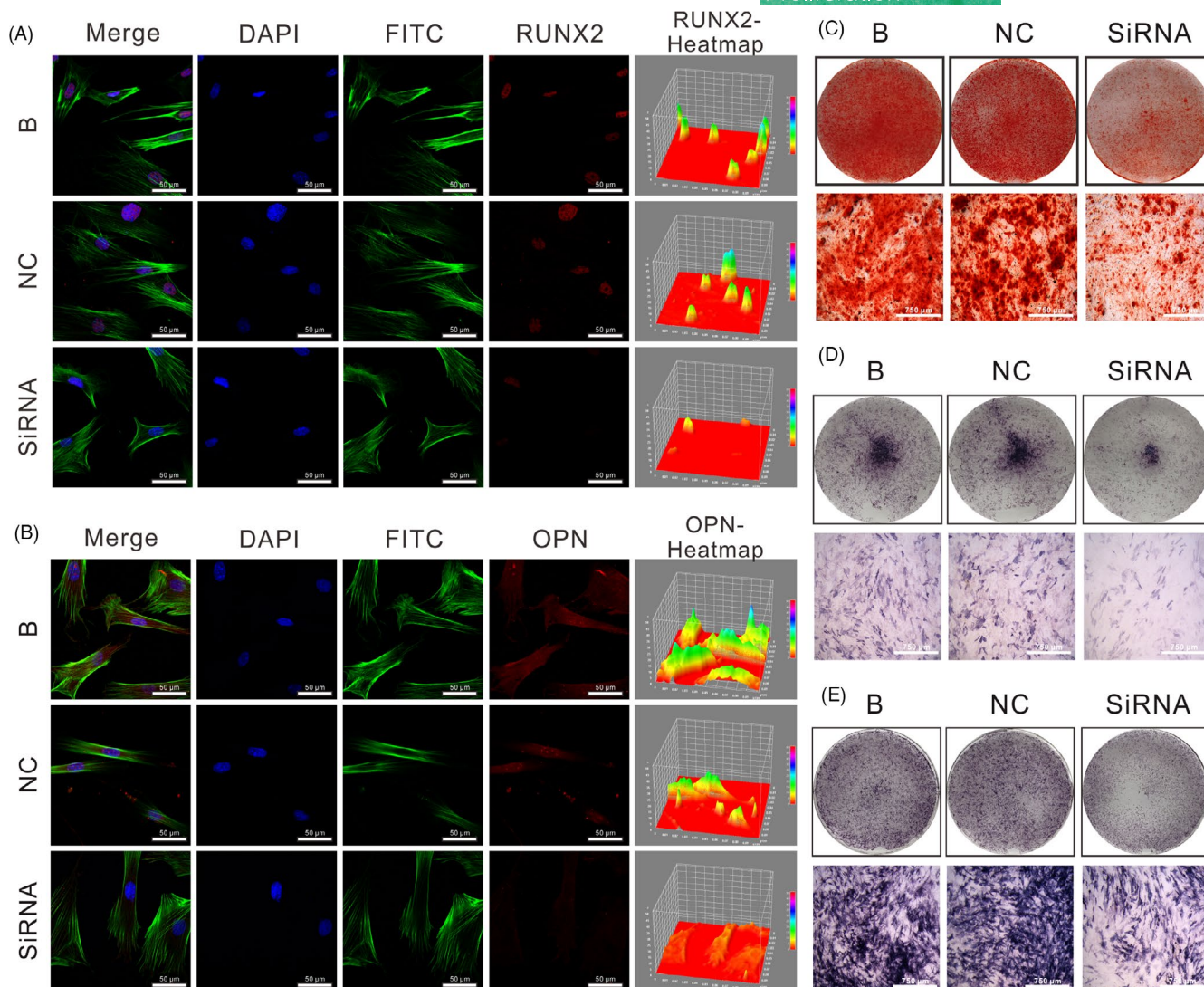


FIGURE 5 AK137033 silencing reduces the osteogenic differentiation potential of CON-ASCs. A, B, At 3 days after osteogenic induction, immunofluorescence staining of RUNX2 and OPN proteins was performed in CON-ASCs. C, Alizarin red staining showed that the bone differentiation potential of the SiRNA group was decreased compared to that of B and NC groups after 14 days of osteogenesis induction in CON-ASCs. At 3 (D) or 5 (E) days of osteogenic induction in CON-ASCs, ALP staining showed that alkaline phosphatase activity of the SiRNA group was lower than that of B and NC groups

groups at 14 days of osteogenesis (Figure 7C). ALP staining revealed higher production of alkaline phosphatase in the OE group than that in B and NC groups at 3 and 5 days of osteogenic induction (Figure 7D, E). These changes indicated that overexpression of AK137033 enhanced the osteogenic differentiation potential of DOP-ASCs.

3.9 | In vivo verification of AK137033 in regulating the osteogenic ability of ASCs

To further assess the osteogenic role of AK137033 in vivo, we knocked down AK137033 in CON-ASCs using a specific shRNA lentivirus (shRNA group) and overexpressed AK137033 in DOP-ASCs through a specific LVRNA lentivirus (LVRNA group). After lentivirus infection, the effect was assessed by qPCR and western blotting

after 3 days of osteogenic induction. The results showed that the shRNA lentivirus knocked down the expression of AK137033 in CON-ASCs and the LVRNA lentivirus overexpressed AK137033 in DOP-ASCs (Figure 8A, B). Next, we prepared ASC-seeded BCP scaffolds. Scanning electron microscopy and fluorescence microscopy showed that CON-ASCs and DOP-ASCs adhered to the surface and pores of BCP scaffolds (Figure 8C).

Subsequently, we implanted ASC-seeded BCP scaffolds into a critical-sized calvarial bone defect model in CON and DOP mice (Figure 8D). Among them, CON mice were implanted with a BCP scaffold seeded with CON-ASCs (CON-B), BCP scaffold seeded with CON-ASCs transfected with the knockdown lentivirus vector (CON-NC), and BCP scaffold seeded with CON-ASCs with AK137033 knockdown (CON-shRNA); and BCP scaffold seeded with DOP-ASCs (DOP-B), BCP scaffold seeded with DOP-ASCs infected with the overexpression

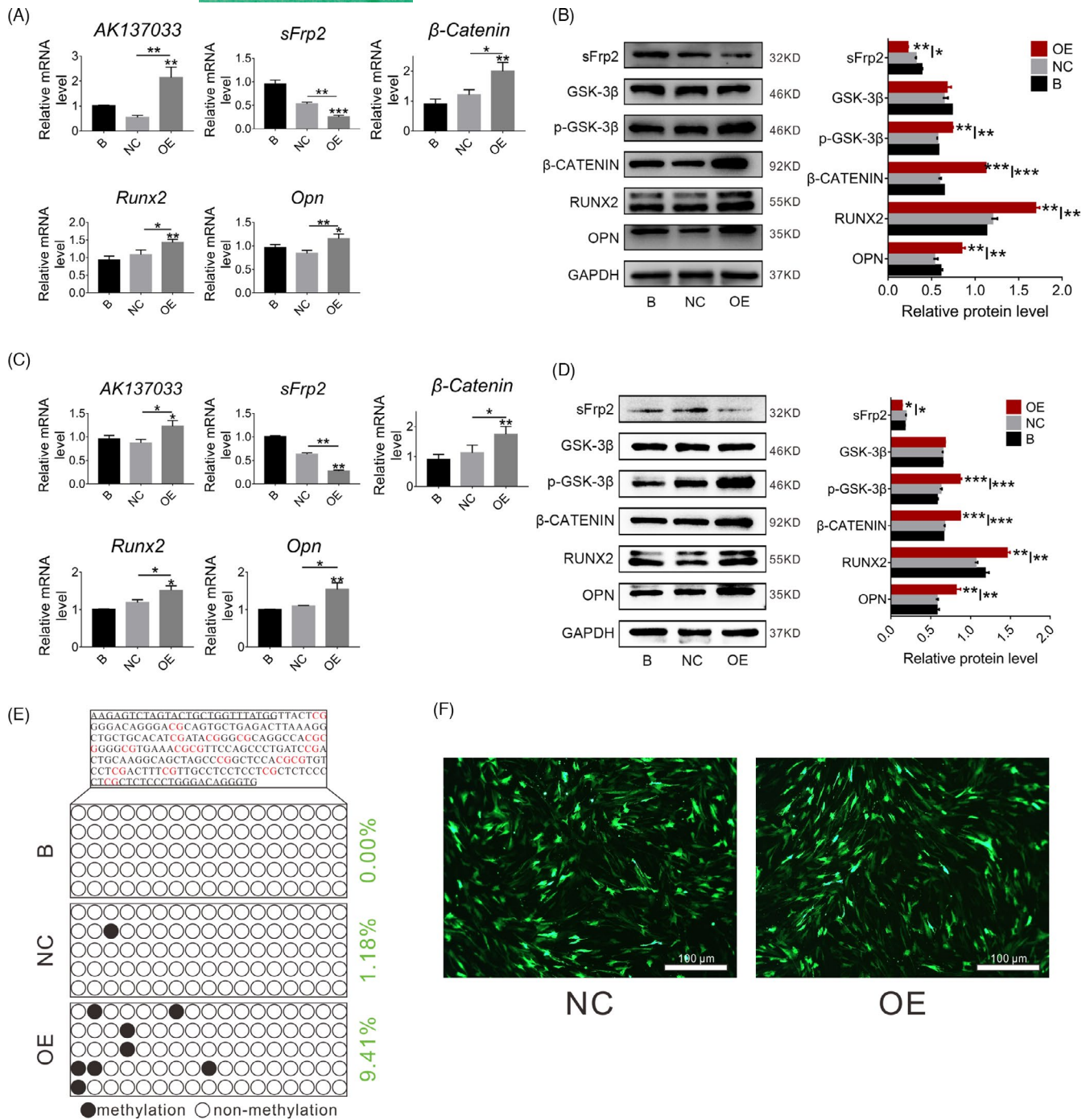


FIGURE 6 AK137033 overexpression activates the Wnt signaling pathway in DOP-ASCs by increasing the DNA methylation level of the sFrp2 promoter region. A, B, The mRNA and protein levels of Wnt signaling pathway makers and osteogenesis-related molecules in the OE group were increased after AK137033 overexpression in DOP-ASCs (osteoinduction for 3 days). C, D, After AK137033 overexpression in DOP-ASCs, the mRNA and protein levels of Wnt signaling pathway markers and osteogenesis-related molecules were increased in the OE group (osteoinduction for 6 days). E, BSP results revealed that the DNA methylation level of the sFrp2 promoter region in the OE group was upregulated compared to that in B and NC groups. F, Cellular uptake of NC and OE plasmids by DOP-ASCs after treatment for 48 h. Data shown as the mean \pm SD ($n \geq 3$), * $p < 0.05$; ** $p < 0.01$; *** $p < 0.001$

lentivirus vector (DOP-NC), and BCP scaffold seeded with DOP-ASCs that overexpressed AK137033 (DOP-LVRNA) were implanted in DOP mice. At 8 weeks after transplantation, the formation of mouse calvarial bone was detected by micro-CT and histochemistry. Micro-CT scanning showed that the knockout of AK137033 decreased the bone

volume/total volume (Tb.BV/TV) and trabecular thickness (Tb.Th) in CON mice, while the bone surface area/bone volume (Tb.BS/BV) was increased. Conversely, in DOP mice, overexpression of AK137033 reversed the decrease in bone formation caused by DOP (Figure 9A, B). In CON mice, histochemical staining revealed that the amount of

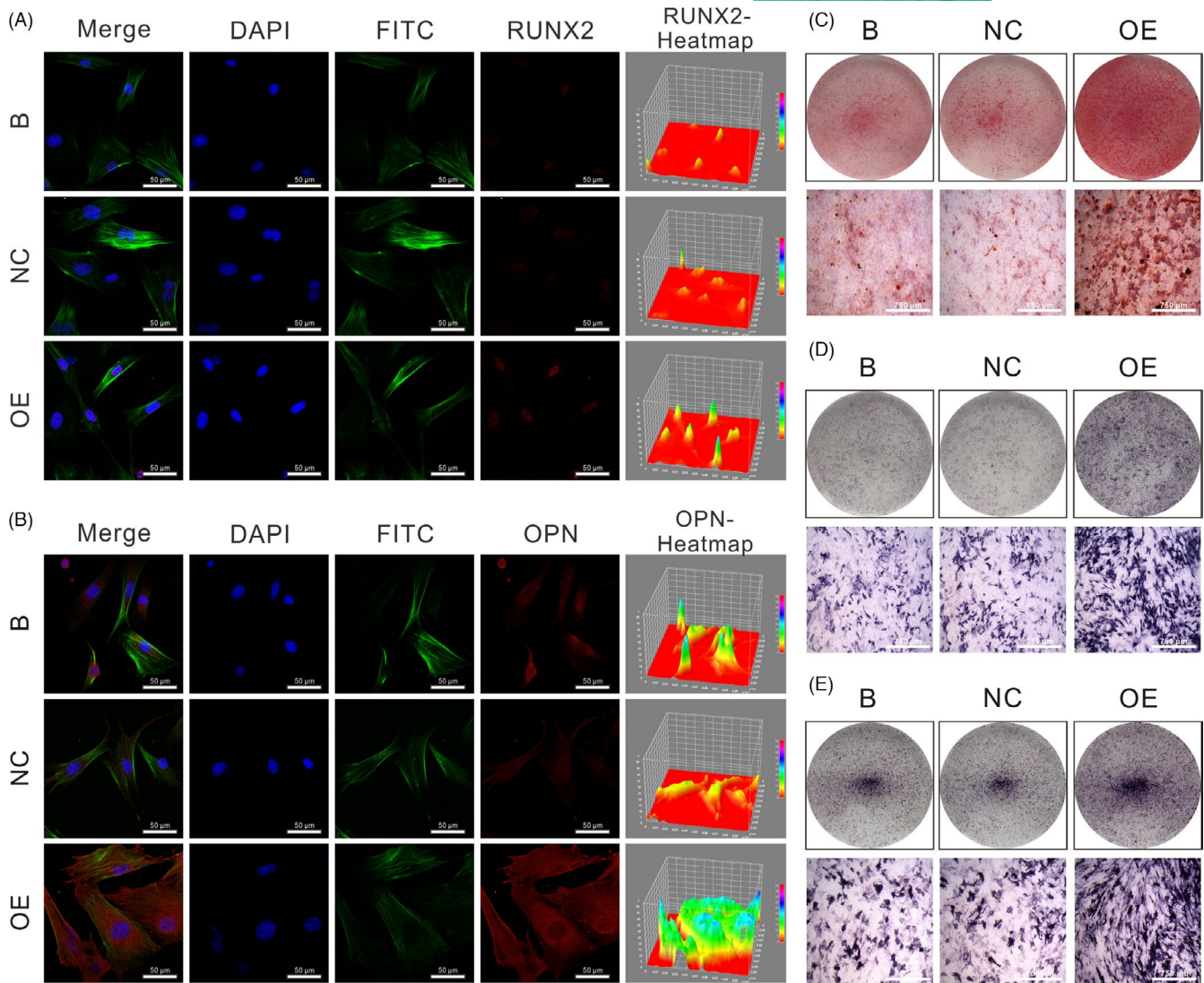


FIGURE 7 AK137033 overexpression increases the osteogenic ability of DOP-ASCs. A, B, At 3 days after osteogenic induction, immunofluorescence staining of RUNX2 and OPN proteins was performed in DOP-ASCs. C, AK137033 overexpression rescued the decline of the osteogenic ability of DOP-ASCs induced by DOP as determined by alizarin red staining (14 days of osteogenic induction). At 3 (D) or 5 (E) days of osteogenic induction in DOP-ASCs, ALP staining showed that alkaline phosphatase activity in the OE group was higher than that in B and NC groups

fibrotic and mineralized new bone in the shRNA group was less than that in B and NC groups. In DOP mice, the bone formation ability of the LVRNA group was rescued compared to that in B and NC groups (Figure 9C, D). On the basis of these results, we concluded that AK137033 regulated osteogenesis of ASCs *in vivo*. The decrease in the osteogenic differentiation potential of DOP-ASCs was related to the low expression of AK137033.

4 | DISCUSSION

Diabetes is a group of systemic metabolic diseases characterized by a disturbance in carbohydrate metabolism caused by islet dysfunction or insulin resistance.³¹ Chronic hyperglycemia causes chronic damage to various tissues and organs of the body, which results in

various diabetic complications, especially in the eyes, kidneys, blood vessels, and bones.^{32–34} Among them, diabetic osteoporosis refers to the metabolic bone disease that occurs because of the hyperglycemic microenvironment.³² Recent studies have shown that insulin deficiency or tolerance in diabetic patients leads to disruptions of glucose, lipid, and calcium metabolisms, which results in dysfunctional osteoblasts and osteoclasts and ultimately causes systemic bone loss and a reduction in bone mineral density.^{35,36} Additionally, hyperglycemic microenvironment-induced autophagy adversely affects the proliferation and differentiation of osteoblasts, which is associated with increases in fracture risk and bone mineral density loss in diabetes.³⁷ However, there are few studies on the role of epigenetic alterations of ASCs in the pathogenesis of DOP. The etiology and course of DOP are complex. Therefore, establishment of a DOP animal model is crucial to study the pathogenesis, prevention, and

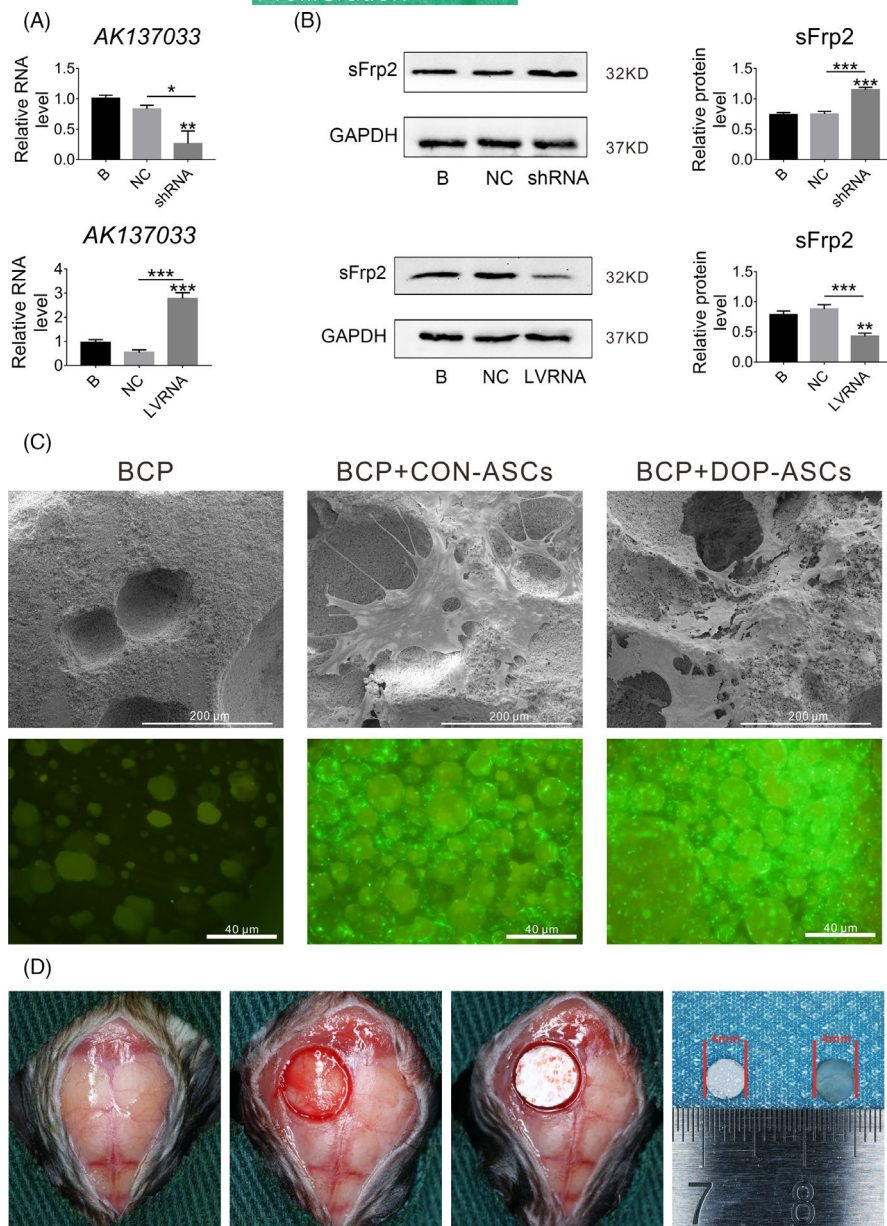


FIGURE 8 Preparation of ASC-seeded BCP scaffolds and the critical-sized calvarial bone defect mouse model. A, B, Transfection efficiency verified by qPCR and western blot analysis after CON-ASCs were infected with the shRNA lentivirus, and DOP-ASCs were infected with LVRNA. C, Scanning electron microscopy and fluorescence microscopy of prepared CON-ASC-seeded BCP scaffolds and DOP-ASC-seeded BCP scaffolds. D, Establishment of the critical-sized calvarial bone defect mouse model and implantation of ASC-seeded BCP scaffolds. Data shown as the mean \pm SD ($n \geq 3$), * $p < 0.05$; ** $p < 0.01$; *** $p < 0.001$

treatment of DOP. STZ injection is considered to be one of the most common methods to establish a DOP animal model.³⁸ In this study, we established DOP model mice by injecting STZ. After injection, the DOP group had a steady increase in blood glucose and showed typical diabetic symptoms of increased water and food intake, micturition, and weight loss. Subsequently, the results of histochemical staining and micro-CT revealed fewer and disordered bone trabeculae in the DOP group compared to those in the CON group, and the bone cortex had become thinner. Therefore, we concluded that the DOP mouse model was established successfully. Next, we isolated and cultured CON-ASCs and DOP-ASCs to explore the molecular mechanism by which AK137033 affects osteogenesis of DOP-ASCs via DNA methylation.

The Wnt signaling pathway plays an important role in the differentiation and development of stem cells because of high conservation, structural complexity, and the ability of the developmental

cascade to integrate the signals of other pathways.³⁹ The canonical Wnt pathway (Wnt/ β -catenin) and noncanonical Wnt pathway (Wnt/PCP and Wnt/ Ca^{2+}) affect bone modeling and reconstruction by regulating the energy metabolism and osteogenesis of osteoblasts.⁴⁰⁻⁴³ sFrp2 is an antagonist of the canonical Wnt pathway. It binds to Wnt ligands through a cysteine-rich domain or C-terminal netrin-like domain, or forms nonfunctional complexes with frizzles-related receptors to inhibit Wnt signaling.⁴⁴ As a crucial molecule of the Wnt signaling pathway, sFrp2 regulates the proliferation, apoptosis, and differentiation of stem cells by inhibiting the Wnt signaling pathway to be involved in multiple biological processes such as cardiac malformations and cardiovascular diseases,⁴⁵ the regulation of skin and hair follicle development,⁴⁶ and the occurrence, development, and prognosis of gastric cancer.⁴⁷ However, no study has revealed the specific role of sFrp2 in regulating the osteogenic potential of DOP-ASCs through

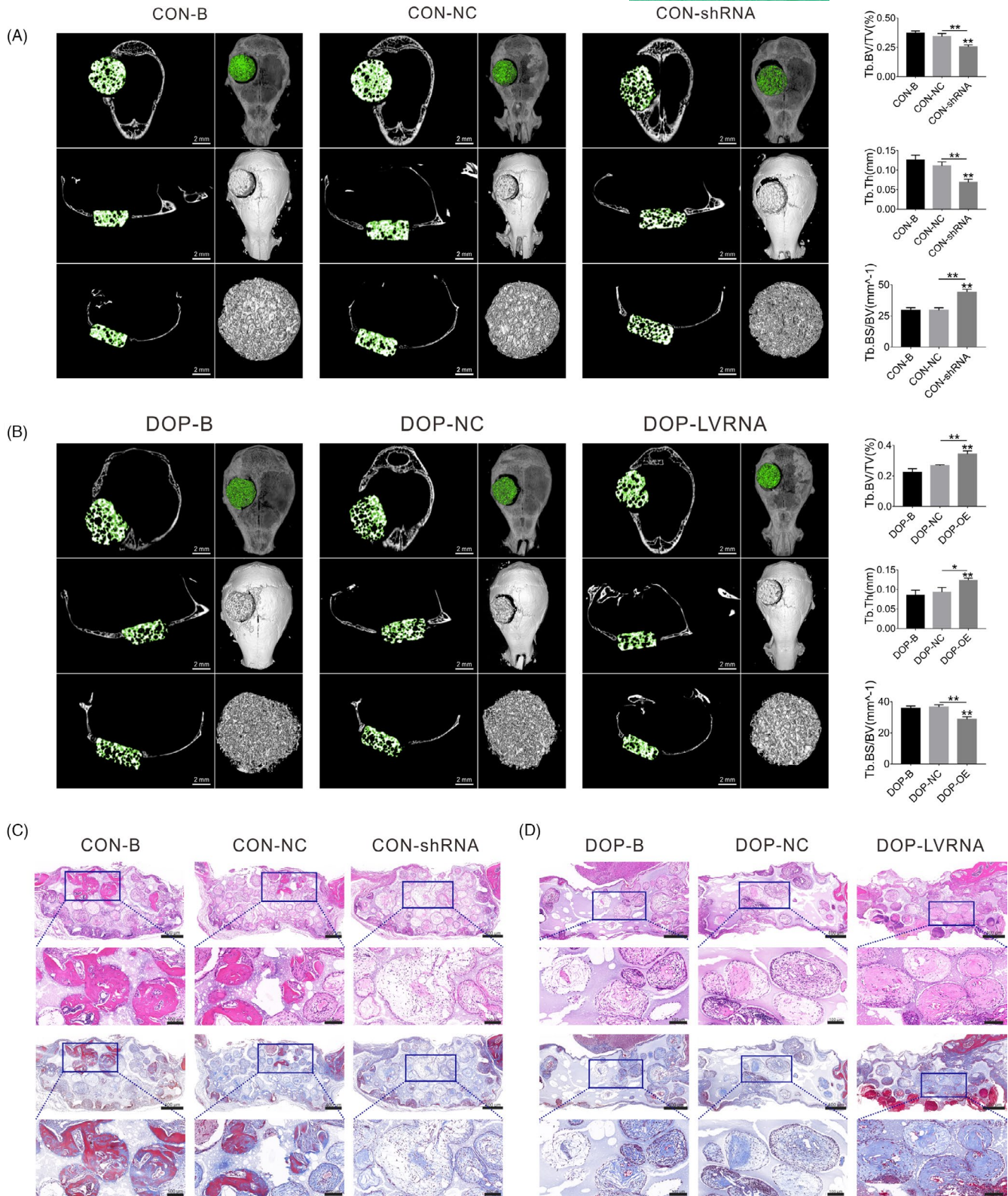


FIGURE 9 Evaluation of skull repair at 8 weeks after implantation. A, B, Micro-CT scanning showed that the knockout of AK137033 decreased Tb.BV/TV and Tb. Th, while Tb.BS/BV was increased in CON mice. In DOP mice, overexpression of AK137033 reversed the decreases in Tb.BV/TV and Tb. Th, and the increased Tb.BS/BV caused by DOP. C, D, H&E and Masson's staining showed that, in CON mice, the amount of fibrotic and mineralized new bone in the shRNA group was less than that in B and NC groups. In DOP mice, the bone formation ability of the LVRNA group was rescued compared with B and NC groups. Data shown as the mean \pm SD ($n \geq 3$), * $p < 0.05$; ** $p < 0.01$; *** $p < 0.001$

the Wnt signaling pathway. In the present study, we performed mRNA/LncRNA expression profiling and MeDIP sequencing of CON-ASCs and DOP-ASCs. The results showed a significant difference in the DNA methylation level of the sFrp2 promoter region in the two groups, which was related to LncRNA-AK137033. Moreover, we verified the AK137033 expression level, Wnt signaling pathway difference, and osteogenic differentiation potential of CON-ASCs and DOP-ASCs *in vitro*. The results showed that, compared with CON-ASCs, the AK137033 expression level, Wnt signaling pathway, and osteogenic differentiation potential were inhibited in DOP-ASCs. Moreover, Meth Primer analysis and BSP results demonstrated that the methylation degree of CON-ASCs was higher than that of matched DOP-ASCs in the sFrp2 promoter region. The above results supported the mRNA/LncRNA expression profiling and MeDIP sequencing results. However, further functional studies are needed to demonstrate the relationship between the DNA methylation level of the sFrp2 promoter region and AK137033.

LncRNAs are a kind of long-chain RNA (more than 500 nt) that lacks a protein-coding ability.^{48,49} There is increasing evidence of the roles of LncRNAs in many important biological processes that include gene transcription, mRNA shearing, cell cycle control, epigenetic regulation, and cellular immunity.⁵⁰⁻⁵² Recent studies have shown that LncRNAs regulate local and distal gene expression at their transcriptional location through multiple mechanisms that include functioning as competing endogenous RNA or acting as monomers with specific domains and recruiting specific DNAs, RNAs, or proteins to regulate downstream gene expression.⁵³ DNA methylation refers to modification of specific DNA fragments mediated by DNA methyltransferase families, which results in methylation of the fifth carbon atom on dinucleotide cytosine in CpG islands.^{54,55} DNA methylation in the promoter region inhibits gene expression by recruiting transcription barriers, and DNA methylation in the gene body regulates gene transcription by selective splicing of transcripts or stability of the genome.⁵⁶ As an important part of epigenetics, the association between DNA methylation and LncRNA expression is called LncRNA expression quantitative trait methylation (Lnc-eQTM).⁵⁷ A growing number of studies have conducted in-depth research on Lnc-eQTMs. Geng et al. found that Lnc-MAP3K13-7:1 inhibits the proliferation of ovarian granulosa cells in polycystic ovary syndrome through DNMT1-mediated hypomethylation of the CDKN1A promoter.⁵⁸ Zheng et al. demonstrated that Lnc-AK001058 promotes the proliferation, migration, and invasion of colorectal cancer cells by regulating methylation of the ADAMTS12 promoter.⁵⁹ In this study, silencing AK137033 in CON-ASCs decreased the DNA methylation level in the sFrp2 promoter region, inhibited the Wnt signaling pathway, and suppressed the osteogenic differentiation potential of CON-ASCs. Additionally, overexpression of AK137033 in DOP-ASCs increased the DNA methylation level in the sFrp2 promoter region, activated the Wnt signaling pathway, and restored the osteogenic differentiation potential of DOP-ASCs. Interestingly,

mRNA/LncRNA expression profiling and MeDIP sequencing of CON-ASCs and DOP-ASCs also showed that the difference in the DNA methylation level of the sFrp2 promoter region between the two groups was related to LncRNA-AK137033. These results suggest that AK137033 inhibits the osteogenic potential of DOP-ASCs by regulating the DNA methylation level in the sFrp2 promoter region.

Studies have shown that the diameter of a mouse calvarial bone defect that cannot heal itself is 4 mm.^{60,61} To further assess the osteogenic role of AK137033 *in vivo*, a critical-sized calvarial bone defect model in mice was established and ASC-seeded BCP scaffolds were implanted. At 8 weeks after transplantation, micro-CT and histochemistry showed that the knockdown of AK137033 reduced bone formation in CON mice and overexpression of AK137077 rescued the reduced bone formation ability of DOP mice caused by the hyperglycemic microenvironment. Therefore, we conclude that AK137033 regulates osteogenesis of ASCs *in vivo*.

In summary, *in vitro* and *in vivo* experiments demonstrated that LncRNA-AK137033 regulates the osteogenic potential of DOP-ASCs by modulating the Wnt signaling pathway via DNA methylation in the sFrp2 promoter region. Our study provides an epigenetic explanation for the regulatory mechanism of the osteogenic potential in DOP-ASCs and is an important reference for the treatment of bone defects in DOP patients.

ACKNOWLEDGEMENTS

This work was supported by National Natural Science Foundation of China (81870746, 81771125), open project of the State Key Laboratory of Oral Disease Research (SKLOD2021OF08), joint project of Luzhou Municipal People's Government and Southwest Medical University (2020LZXNYDZ09), project of Science & Technology Department of Sichuan Province (2018JY0399), and youth science climbing program of The Affiliated Stomatology Hospital of Southwest Medical University (2021KQ01).

CONFLICT OF INTEREST

The authors declare that there are no competing interests.

AUTHOR CONTRIBUTIONS

All authors have made important contributions to this study. Shuanglin Peng conducted *in vitro* and *in vivo* experiments, sorted and analyzed the data, and wrote the main manuscript. Yujin Gao established the diabetic osteoporosis mouse model and cultured CON-ASCs and DOP-ASCs. Sirong Shi completed mRNA/LncRNA expression profiling, MeDIP sequencing, and *in vitro* validation experiments. Dan Zhao carried out *in vitro* experiments and data collection. Huayue Cao and Ting Fu assisted in the *in vivo* experiments. Xiaoxiao Cai designed the study and revised the manuscript. Jingang Xiao conceived and initiated the study, analyzed the data, and provided funding. All authors have read and approved the manuscript.

DATA AVAILABILITY STATEMENT

All data included in this article can be obtained from corresponding author upon reasonable requirements.

ORCID

Xiaoxiao Cai  <https://orcid.org/0000-0002-5654-7414>

Jingang Xiao  <https://orcid.org/0000-0003-1300-7191>

REFERENCES

- Schwartz AV, Pavo I, Alam J, et al. Teriparatide in patients with osteoporosis and type 2 diabetes. *Bone*. 2016;91:152-158.
- Wang JF, Lee MS, Tsai TL, et al. Bone morphogenetic protein-6 attenuates type 1 diabetes mellitus-associated bone loss. *Stem Cells Transl Med*. 2019;8:522-534.
- Gilbert MP, Pratley RE. The impact of diabetes and diabetes medications on bone health. *Endocr Rev*. 2015;36:194-213.
- Xie B, Chen S, Xu Y, et al. The impact of glucagon-like peptide 1 receptor agonists on bone metabolism and its possible mechanisms in osteoporosis treatment. *Front Pharmacol*. 2021;12:697442.
- Goldshtein I, Nguyen AM, dePapp AE, et al. Epidemiology and correlates of osteoporotic fractures among type 2 diabetic patients. *Arch Osteoporos*. 2018;13:15.
- Chahal S, Kumar A, Hussian FSJ. Development of biomimetic electrospun polymeric biomaterials for bone tissue engineering. A review. *J Biomater Sci Polym Ed*. 2019;30:1308-1355.
- Zhang M, Li Y, Rao P, et al. Blockade of receptors of advanced glycation end products ameliorates diabetic osteogenesis of adipose-derived stem cells through DNA methylation and Wnt signalling pathway. *Cell Prolif*. 2018;51:e12471.
- Li Y, Wang L, Zhang M, et al. Advanced glycation end products inhibit the osteogenic differentiation potential of adipose-derived stem cells by modulating Wnt/beta-catenin signalling pathway via DNA methylation. *Cell Prolif*. 2020;53:e12834.
- Kar S, Jasuja H, Katti DR, et al. Wnt/beta-catenin signaling pathway regulates osteogenesis for breast cancer bone metastasis: experiments in an in vitro nanoclay scaffold cancer testbed. *ACS Biomater Sci Eng*. 2020;6:2600-2611.
- Han L, Gong S, Wang R, et al. Knockdown of POSTN inhibits osteogenic differentiation of mesenchymal stem cells from patients with steroid-induced osteonecrosis. *Front Cell Dev Biol*. 2020;8:606289.
- Shen G, Ren H, Shang Q, et al. Foxf1 knockdown promotes BMSC osteogenesis in part by activating the Wnt/beta-catenin signalling pathway and prevents ovariectomy-induced bone loss. *EBioMedicine*. 2020;52:102626.
- Morgan AE, Davies TJ, Mc Auley MT. The role of DNA methylation in ageing and cancer. *Proc Nutr Soc*. 2018;77:412-422.
- Ishihara T, Hickford D, Shaw G, et al. DNA methylation dynamics in the germline of the marsupial tammar wallaby, *Macropus eugenii*. *DNA Res*. 2019;26:85-94.
- Zhan Y, Guo Z, Zheng F, et al. Reactive oxygen species regulate miR-17-5p expression via DNA methylation in paraquat-induced nerve cell damage. *Environ Toxicol*. 2020;35:1364-1373.
- Garcia-Gomez A, Li T, de la Calle-Fabregat C, et al. Targeting aberrant DNA methylation in mesenchymal stromal cells as a treatment for myeloma bone disease. *Nat Commun*. 2021;12:421.
- Reppe S, Lien TG, Hsu YH, et al. Distinct DNA methylation profiles in bone and blood of osteoporotic and healthy postmenopausal women. *Epigenetics*. 2017;12:674-687.
- Peng S, Shi S, Tao G, et al. JKAMP inhibits the osteogenic capacity of adipose-derived stem cells in diabetic osteoporosis by modulating the Wnt signaling pathway through intragenic DNA methylation. *Stem Cell Res Ther*. 2021;12:120.
- Consortium EP, Birney E, Stamatoyannopoulos JA, et al. Identification and analysis of functional elements in 1% of the human genome by the ENCODE pilot project. *Nature*. 2007;447:799-816.
- Quinn JJ, Chang HY. Unique features of long non-coding RNA biogenesis and function. *Nat Rev Genet*. 2016;17:47-62.
- Song S, Liu S, Wei Z, et al. Identification of an immune-related long noncoding RNA pairs model to predict survival and immune features in gastric cancer. *Front Cell Dev Biol*. 2021;9:726716.
- Dong J, Liu J, Wen Y, et al. Down-regulation of Lnc-CYP7A1-1 rejuvenates aged human mesenchymal stem cells to improve their efficacy for heart repair through SYNE1. *Front Cell Dev Biol*. 2020;8:600304.
- Li M, Cong R, Yang L, et al. A novel lncRNA LNC_000052 leads to the dysfunction of osteoporotic BMSCs via the miR-96-5p-PIK3R1 axis. *Cell Death Dis*. 2020;11:795.
- Merry CR, Forrest ME, Sabers JN, et al. DNMT1-associated long non-coding RNAs regulate global gene expression and DNA methylation in colon cancer. *Hum Mol Genet*. 2015;24:6240-6253.
- Sarkar D, Leung EY, Baguley BC, et al. Epigenetic regulation in human melanoma: past and future. *Epigenetics*. 2015;10:103-121.
- Qi X, Yu XJ, Wang XM, et al. Knockdown of KCNQ1OT1 suppresses cell invasion and sensitizes osteosarcoma cells to CDDP by upregulating DNMT1-Mediated Kcnq1 expression. *Mol Ther Nucleic Acids*. 2019;17:804-818.
- Zhao Y, Pan J, Cao C, et al. RNF20 affects porcine adipocyte differentiation via regulation of mitotic clonal expansion. *Cell Prolif*. 2021;54:e13131.
- Shi S, Tian T, Li Y, et al. Tetrahedral framework nucleic acid inhibits chondrocyte apoptosis and oxidative stress through activation of autophagy. *ACS Appl Mater Interfaces*. 2020;12:56782-56791.
- Zhou M, Gao S, Zhang X, et al. The protective effect of tetrahedral framework nucleic acids on periodontium under inflammatory conditions. *Bioact Mater*. 2021;6(6):1676-1688.
- Zhao D, Liu M, Li J, et al. Angiogenic aptamer-modified tetrahedral framework nucleic acid promotes angiogenesis in vitro and in vivo. *ACS Appl Mater Interfaces*. 2021;13:29439-29449.
- Zhang M, Zhang X, Tian T, et al. Anti-inflammatory activity of curcumin-loaded tetrahedral framework nucleic acids on acute gouty arthritis. *Bioact Mater*. 2022;8:368-380.
- Cho J, Scragg R, Petrov MS. Risk of mortality and hospitalization after post-pancreatitis diabetes mellitus vs type 2 diabetes mellitus: a population-based matched cohort study. *Am J Gastroenterol*. 2019;114:804-812.
- Sundbom M, Franzen S, Ottosson J, et al. Superior socioeconomic status in patients with type 2 diabetes having gastric bypass surgery: a case-control analysis of 10 642 individuals. *BMJ Open Diabetes Res Care*. 2020;8:e000989.
- Karim L, Bouxsein ML. Effect of type 2 diabetes-related non-enzymatic glycation on bone biomechanical properties. *Bone*. 2016;82:21-27.
- Rachner TD, Khosla S, Hofbauer LC. Osteoporosis: now and the future. *The Lancet*. 2011;377:1276-1287.
- Murray CE, Coleman CM. Impact of diabetes mellitus on bone health. *Int J Mol Sci*. 2019;20:4873.
- Hofbauer LC, Brueck CC, Singh SK, et al. Osteoporosis in patients with diabetes mellitus. *J Bone Miner Res*. 2007;22:1317-1328.
- Jiang Y, Luo W, Wang B, et al. 1 α ,25-Dihydroxyvitamin D₃ ameliorates diabetes-induced bone loss by attenuating FoxO1-mediated autophagy. *J Biol Chem*. 2021;296:100287.
- Yuan X, Ni H, Chen X, et al. Identification of therapeutic effect of glucagon-like peptide 1 in the treatment of STZ-induced diabetes mellitus in rats by restoring the balance of intestinal flora. *J Cell Biochem*. 2018;119:10067-10074.
- MacDonald BT, Tamai K, He X. Wnt/beta-catenin signaling: components, mechanisms, and diseases. *Dev Cell*. 2009;17:9-26.

40. Baron R, Kneissel M. WNT signaling in bone homeostasis and disease: from human mutations to treatments. *Nat Med*. 2013;19:179-192.
41. Yu AX, Xu ML, Yao P, et al. Corylin, a flavonoid derived from *Psoralea Fructus*, induces osteoblastic differentiation via estrogen and Wnt/ β -catenin signaling pathways. *FASEB J*. 2020;34:4311-4328.
42. Giuliani C. The flavonoid quercetin induces AP-1 activation in FRTL-5 thyroid cells. *Antioxidants (Basel)*. 2019;8:112.
43. Li S, Liu Y, Tian T, et al. Bioswitchable delivery of microRNA by framework nucleic acids: application to bone regeneration. *Small*. 2021;29:e2104359.
44. Wu Y, Liu X, Zheng H, et al. Multiple roles of SFRP2 in cardiac development and cardiovascular disease. *Int J Biol Sci*. 2020;16:730-738.
45. Fan J, Zhang Y, Mu J, et al. TET1 exerts its anti-tumor functions via demethylating DACT2 and SFRP2 to antagonize Wnt/ β -catenin signaling pathway in nasopharyngeal carcinoma cells. *Clin Epigenetics*. 2018;10:103.
46. Zhao B, Chen Y, Yang N, et al. miR-218-5p regulates skin and hair follicle development through Wnt/ β -catenin signaling pathway by targeting SFRP2. *J Cell Physiol*. 2019;234:20329-20341.
47. Wang H, Duan XL, Qi XL, et al. Concurrent hypermethylation of SFRP2 and DKK2 activates the Wnt/ β -catenin pathway and is associated with poor prognosis in patients with gastric cancer. *Mol Cells*. 2017;40:45-53.
48. Kamel LM, Atef DM, Mackawy AMH, et al. Circulating long non-coding RNA GAS5 and SOX2OT as potential biomarkers for diagnosis and prognosis of non-small cell lung cancer. *Biotechnol Appl Biochem*. 2019;66:634-642.
49. Wang C, Jiang X, Li X, et al. Long noncoding RNA HULC accelerates the growth of human liver cancer stem cells by upregulating CyclinD1 through miR675-PKM2 pathway via autophagy. *Stem Cell Res Ther*. 2020;11:8.
50. Wang X, Liu C, Zhang S, et al. N(6)-methyladenosine modification of MALAT1 promotes metastasis via reshaping nuclear speckles. *Dev Cell*. 2021;56(5):702-715.e8. 10.1016/j.devcel.2021.01.015
51. Xie X, Lin J, Fan X, et al. LncRNA CDKN2B-AS1 stabilized by IGF2BP3 drives the malignancy of renal clear cell carcinoma through epigenetically activating NUF2 transcription. *Cell Death Dis*. 2021;12:201.
52. Wu R, Wang L, Yin R, et al. Epigenetics/epigenomics and prevention by curcumin of early stages of inflammatory-driven colon cancer. *Mol Carcinog*. 2020;59:227-236.
53. Kato M, Natarajan R. Epigenetics and epigenomics in diabetic kidney disease and metabolic memory. *Nat Rev Nephrol*. 2019;15:327-345.
54. Plumptre L, Tammen SA, Sohn KJ, et al. Maternal and cord blood folate concentrations are inversely associated with fetal DNA hydroxymethylation, but not DNA methylation, in a cohort of pregnant Canadian women. *J Nutr*. 2020;150:202-211.
55. Skvortsova K, Stirzaker C, Taberlay P. The DNA methylation landscape in cancer. *Essays Biochem*. 2019;63:797-811.
56. Jones PA. Functions of DNA methylation: islands, start sites, gene bodies and beyond. *Nat Rev Genet*. 2012;13:484-492.
57. Wu X, Gao Y, Bu J, et al. Identification of potential long non-coding RNA expression quantitative trait methylations in lung adenocarcinoma and lung squamous carcinoma. *Front Genet*. 2020;11:602035.
58. Geng X, Zhao J, Huang J, et al. lnc-MAP3K13-7:1 inhibits ovarian GC proliferation in PCOS via DNMT1 downregulation-mediated CDKN1A promoter hypomethylation. *Mol Ther*. 2021;29(3):1279-1293. 10.1016/j.yymthe.2020.11.018
59. Zheng S, Lin F, Zhang M, et al. AK001058 promotes the proliferation and migration of colorectal cancer cells by regulating methylation of ADAMTS12. *Am J Transl Res*. 2019;11:5869-5878.
60. Swanson WB, Zhang Z, Xiu K, et al. Scaffolds with controlled release of pro-mineralization exosomes to promote craniofacial bone healing without cell transplantation. *Acta Biomater*. 2020;118:215-232.
61. Fan J, Lee CS, Kim S, et al. Generation of small RNA-modulated exosome mimetics for bone regeneration. *ACS Nano*. 2020;14:11973-11984.

How to cite this article: Peng S, Gao Y, Shi S, et al. LncRNA-AK137033 inhibits the osteogenic potential of adipose-derived stem cells in diabetic osteoporosis by regulating Wnt signaling pathway via DNA methylation. *Cell Prolif*. 2022;55:e13174. doi:[10.1111/cpr.13174](https://doi.org/10.1111/cpr.13174)